Transition strengths and multiple band structure in ^{82}Sr

S. L. Tabor, J. Döring, J. W. Holcomb, G. D. Johns, T. D. Johnson,* T.J. Petters, M. A. Riley, and P. C. Womble†
Department of Physics, Florida State University, Tallahassee, Florida 32306
(Received 28 September 1993)

High-spin states in ^{82}Sr were studied using the ^{56}Fe(^{29}Si,2pn) reaction at 95 MeV with a thick 78 mg/cm^2 natural Fe (92% ^{56}Fe) target. Prompt γ-γ coincidences were measured using three Compton-suppressed Ge detectors at 90° relative to the beam and two at 30°. Directional correlation of oriented nuclei ratios were determined from the 30° − 90° coincidences to assist in assigning spin changes. Nine new states were found, along with 38 new transitions. The Doppler-shift attenuation method was used to determine the mean lifetimes of 22 states in ^{82}Sr. The continuum side feeding times into 10 states were determined by comparing the decay line shapes in coincidence with transitions above and below the state under study. The average transition quadrupole moment of 2.8(2) e b in the ground-state band of ^{82}Sr would correspond to a relatively large axial quadrupole deformation of $\beta_2 = 0.33$, in agreement with theoretical predictions. The excited 2^+ band has a higher moment of inertia but a lower transition quadrupole moment of 2.4(2) e b. In the negative-parity bands the quadrupole moment falls from about 3 to 2 e b with increasing spin.

PACS number(s): 21.10.Tg, 23.20.−g, 27.50.+e

I. INTRODUCTION

Nuclei in the f-p-g shell are predicted [1] to have some of the highest ground-state deformations, but the relatively low single-particle level density leads to strong interactions between the collective and single-particle degrees of freedom. The Sr isotopes ($Z = 38$) provide some of the best examples of this behavior. Lifetime measurements [2] in the ground-state band (GSB) of ^{78}Sr indicate transition quadrupole moments Q_t of about 4 e b, corresponding to a very large axial quadrupole deformation of $\beta_2 \approx 0.46$. The addition of just three more neutrons leads to a much reduced Q_t value of 2 e b ($\beta_2 \approx 0.24$) in the GSB of ^{81}Sr [3]. However, the shape of ^{81}Sr is very sensitive to the orbital occupied by the odd neutron, changing from oblate to prolate to a strongly deformed prolate shape with $\beta_2 \approx 0.39$ for the [431] $\frac{1}{2}$ Nilsson state arising from the $d_{5/2}$ intruder orbital.

Because of the rich spectrum of shapes and rotational behavior observed in the Sr isotopes, their collective behavior has been investigated in some detail theoretically [4]. These calculations suggest a rather large prolate deformation of $\beta_2 \approx 0.32$ for the GSB of ^{82}Sr even though it is farther from ^{78}Sr and closer to the shell closure at $N = 50$ than ^{81}Sr. A coexisting oblate shape with $\beta_2 \approx 0.27$ was also predicted. Two positive-parity rotational bands are known in ^{82}Sr and the excited band becomes yrast at higher spins. Lifetime measurements in ^{82}Sr would provide a good test of these theoretical shape predictions and of their association with the experimentally observed bands.

The level scheme of ^{82}Sr has been studied for some time with ever increasing sensitivity. The first four members of the ground-state rotational band were reported in Ref. [5] and a number of low-spin states, including the lowest 3^- and (5^-) states and second 0^+ and 2^+ states, were observed in the (p,t) reaction [6]. Two (α, xn) reactions [7,8] extended the GSB to (10^+), explored the excited 2^+ band, and reported the first tentative evidence for a negative-parity band. The band structure of ^{82}Sr was further developed using heavy-ion fusion-evaporation reactions [9,10]. Quasiparticle alignment in the GSB of ^{82}Sr was investigated directly through the measurement of g factors using the transient-field technique [11]. The most recent studies using the Oak Ridge Spin Spectrometer [12,13] and the NORDBALL [14] have extended several bands up to spins ranging from 18 to 29$\hbar$.

Although the level scheme of ^{82}Sr has been investigated by a number of groups, only one measurement of the lifetimes of the low-lying states using the recoil-distance method has been reported [9]. Therefore, the present investigation was designed to measure forward-angle γ-ray line shapes in coincidence to determine mean lifetimes of the higher-lying states using the Doppler-shift attenuation method (DSAM). However, in the process, some questions about the level scheme also had to be resolved. In particular, there has been a considerable variation in the literature concerning the ordering of the 1489, 522, 694, and 876 keV transitions. Fortunately, the excellent statistics obtained in the present experiment allowed the determination of a number of new linking transitions which give direct evidence on the ordering of the decays. A number of new states were also found near the bottom of the bands which has helped to clarify the multiple-band structure in ^{82}Sr. The excellent statistics also allowed a direct determination of side-feeding times by comparing line shapes in coincidence with transitions above and below the one under study. ^{82}Sr was the dominant product of the reaction in this experiment, accounting for about 45% of the total yield. ^{82}Y was produced with about 10% of the yield and was also studied [15].

*Present address: II. Physikalisches Institut, Universität Göttingen, D-37073 Göttingen, Federal Republic of Germany.
†Present address: Oak Ridge National Laboratory, Mail Stop 6388, Oak Ridge, TN 37830.

 ©1994 The American Physical Society

II. EXPERIMENTAL PROCEDURE

The ^{56}Fe(^{29}Si,2pn) reaction at 95 MeV was used to populate high-spin states in ^{82}Sr. The ^{29}Si beam was obtained from the 4.7% isotopic abundance in a sample of natural Si in the inverted sputter source and accelerated with the FSU Tandem-Superconducting LINAC facility. A thick 78 mg/cm^2 natural Fe (92% ^{56}Fe) target was used so that lifetimes could be measured using the DSAM.

Prompt γ-γ coincidences were detected with five 25% efficient [compared to a 7.6 cm by 7.6 cm NaI(Tl) scintillator] Compton-suppressed Ge detectors. Three of the detectors were placed at 90° relative to the beam and two at 30°. About 8×10^7 twofold coincidences were written to tape. The energy calibrations were based on the following lines in the spectra: 96.7 (^{79}Rb), 175.6 (^{80}Rb), 385.7 (^{80}Sr), 511.0(e^+e^-), 754.9 (^{78}Kr), 846.8 (^{56}Fe), 900.7 (^{82}Sr), and 1489.0 (^{82}Sr) keV. The ^{82}Sr energies were taken from Ref. [13] and are consistent with earlier values and the other lines in the fit. A further self-consistency test is that the energies of the ^{82}Sr lines determined in the present work are within 0.1–0.2 keV of the values used in the calibration. The data were then gainshifted to a dispersion of 0.8 keV/channel and sorted into a 90°-90° triangular array and a 30°-90° square array.

The 90° spectra projected from both arrays were used to construct the level scheme. The 30° spectra projected from the square array provided line shapes for the determination of lifetimes using the DSAM. The directional correlation of oriented nuclei (DCO) ratios were determined from the peak areas in the 30°- 90° coincidence array according to

$$R_{\mathrm{DCO}} = \frac{I(\gamma \text{ at } 30^\circ \text{ gated by } \gamma_G \text{ at } 90^\circ)}{I(\gamma \text{ at } 90^\circ \text{ gated by } \gamma_G \text{ at } 30^\circ)}. \quad (1)$$

$E2$ transitions close to the transition of interest were used as gates. In most cases the results from several gates were compared to determine an average value and uncertainty. The DCO ratios for $E2$ transitions are expected [16] to be unity, while those for $\Delta I = 1$ decays depend on the spin, mixing ratio δ, and degree of alignment. For pure $M1$ or $E1$ decays ($\delta = 0$) from states of spin greater than 10$\hbar$, R_{DCO} should be between 0.42 and 0.52 depending on the degree of alignment. This range increases for lower-spin states, and R_{DCO} varies considerably with δ for mixed $M1/E2$ transitions.

III. BAND STRUCTURE IN ^{82}SR

The level scheme of ^{82}Sr as seen in the present work is shown in Fig. 1. Because of the large number of bands,

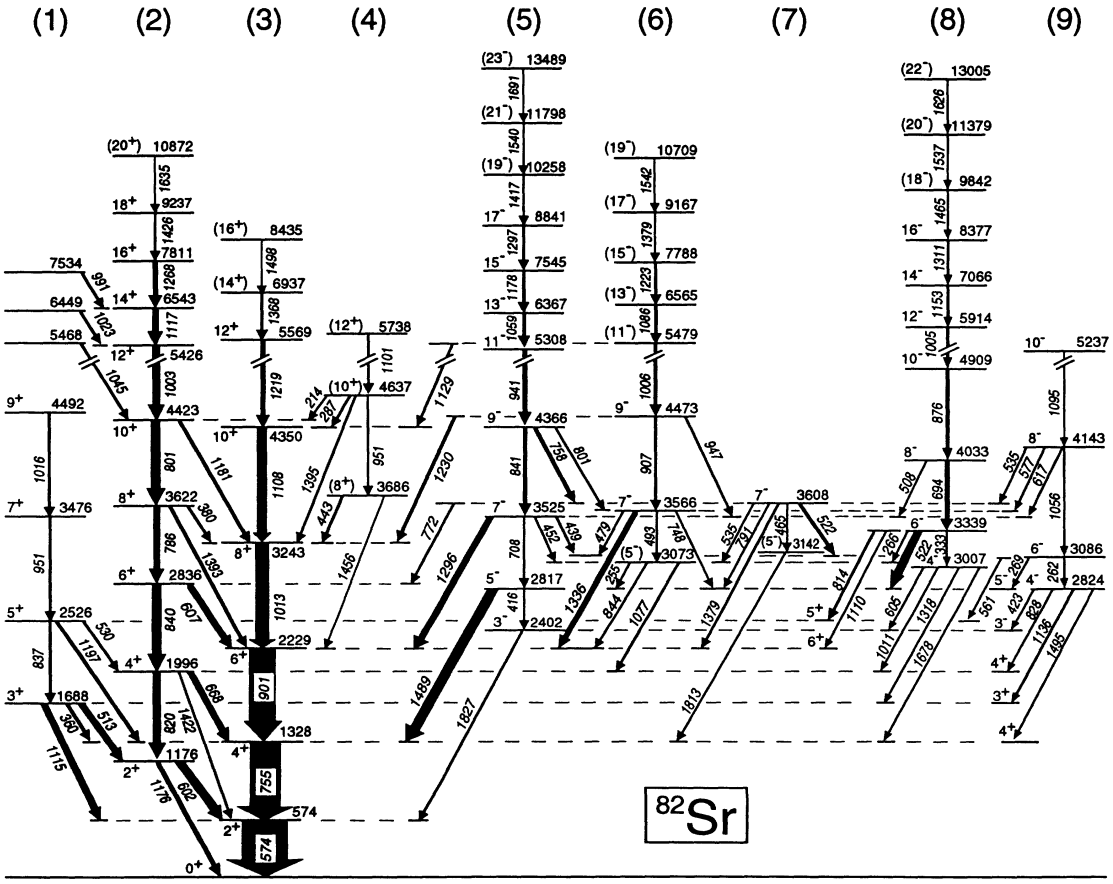

FIG. 1. The level scheme of ^{82}Sr as deduced from the present work. Note that the vertical scale is reduced by a factor of 3 above an excitation energy of 5000 keV and the separation between the three 7$^-$ states has been exaggerated for clarity. The low-lying negative-parity states are strongly mixed, so the horizontal placement of these levels does not necessarily indicate a band assignment. The numbers above the bands are merely serial numbers to aid in the discussion.

we have followed the example of Refs. [12,13] and placed serial numbers above the decay cascades to facilitate the discussion. However, because the bands are arranged differently in Fig. 1, the serial numbers do not correspond to those in Refs. [12,13]. The level and decay information determined in the present work is also presented in Table I. Details about the construction of the level scheme are given below.

TABLE I. Energies, intensities, branching, and DCO ratios of transitions in ^{82}Sr.

E_x (keV)	I_i^π	I_f^π	E_γ(keV)	I_γ	B.R.	R_{DCO}
573.5(1)	2^+	0^+	573.5(1)	100	100	1.04(4)
1175.6(1)	2_2^+	2^+	602.0(1)	25(3)	80.6(8)	0.72(3)
		0^+	1175.7(2)	5.9(10)	19.4(8)	0.84(12)
1328.4(1)	4^+	2^+	754.9(1)	82(4)	100	1.00(7)
1688.4(1)	3^+	4^+	359.9(3)	1.5(5)	4.7(6)	<0.47
		2_2^+	512.9(2)	13.8(20)	42.5(20)	1.14(8)
		2^+	1114.9(1)	17.2(25)	52.8(22)	1.09(3)
1995.9(1)	4_2^+	4^+	667.5(1)	9.9(15)	36.8(10)	0.57(4)
		2_2^+	820.3(1)	16.4(20)	60.6(10)	1.00(3)
		2^+	1422.4(3)	0.8(3)	2.6(4)	
2229.2(1)	6^+	4^+	900.8(1)	54(3)	100	0.96(8)
2401.6(3)	3^-	2^+	1827.0(3)	2.0(7)	100	0.50(7)
2525.5(1)	5^+	4_2^+	529.8(2)	0.9(3)	10.1(14)	0.41(7)
		3^+	837.1(1)	6.8(15)	74.4(26)	1.14(11)
		4^+	1197.1(2)	1.4(4)	15.5(24)	1.25(19)
2817.2(1)	5^-	3^-	415.6(3)	0.4(1)	1.8(4)	
		4^+	1488.8(2)	23(2)	98.2(4)	0.53(2)
2824.2(1)	4^-	3^-	422.6(3)	0.4(1)	5.1(4)	<0.29
		4_2^+	828.4(2)	0.9(2)	13.0(10)	0.84(12)
		3^+	1135.8(1)	5.6(7)	78.0(12)	0.45(2)
		4^+	1494.9(3)	0.3(1)	3.9(6)	0.56(7)
2836.1(1)	6_2^+	6^+	606.9(1)	7.1(6)	26.8(8)	0.71(3)
		4_2^+	840.2(1)	19.4(25)	73.2(8)	0.99(8)
3006.7(2)	4_2^-	3^-	605.1(1)	0.6(2)	28.0(30)	
		4_2^+	1010.7(2)	0.2(1)	9.3(22)	
		3^+	1318.3(3)	1.0(2)	42.9(40)	0.61(9)
		4^+	1677.6(4)	0.4(1)	19.8(36)	0.66(15)
3073.1(2)	(5_2^-)	5^-	255.4(3)	0.1(1)	4.0(8)	
		6^+	843.6(2)	0.9(2)	37.3(30)	0.65(15)
		4_2^+	1077.4(2)	1.4(3)	58.7(32)	0.20(4)
3086.2(1)	6^-	4^-	262.0(1)	2.3(2)	49.6(14)	1.08(9)
		5^-	268.8(1)	1.8(2)	39.7(12)	
		5^+	560.8(2)	0.5(1)	10.7(10)	
3141.7(2)	(5_3^-)	4^+	1812.8(4)	1.3(3)	100	0.77(11)
3242.6(1)	8^+	6^+	1013.4(1)	32(3)	100	1.00(13)
3339.3(1)	6_2^-	(5_2^-)	266.2(2)	0.6(1)	2.7(2)	0.48(6)
		4_2^-	332.5(2)	1.2(3)	5.5(4)	1.12(8)
		5^-	522.1(1)	15.2(18)	69.3(9)	0.21(1)
		5^+	813.9(1)	2.4(5)	11.1(6)	0.61(5)
		6^+	1110.3(2)	2.5(4)	11.4(8)	0.77(7)
3476.1(2)	7^+	5^+	950.6(2)	3.1(7)	100	0.74(11)
3525.4(2)	7^-	6^-	438.9(2)	1.0(2)	7.2(8)	0.39(1)
		(5_2^-)	451.9(3)	0.5(1)	3.6(6)	
		5^-	707.9(2)	0.8(3)	5.2(8)	1.02(15)
		6^+	1296.2(2)	12.3(15)	84.0(12)	0.42(5)
3565.7(2)	7_2^-	6^-	479.3(2)	1.2(4)	13.1(14)	0.38(6)
		(5_2^-)	492.7(4)	0.1(1)	0.7(4)	
		5^-	748.3(2)	1.0(1)	10.7(16)	1.20(13)
		6^+	1336.5(2)	7.1(9)	75.5(20)	0.50(5)
3607.7(2)	7_3^-	(5_3^-)	465.4(2)	1.1(3)	8.6(8)	0.75(1)
		6^-	521.5(2)	3.7(5)	29.9(16)	0.21(5)
		(5_2^-)	534.6(2)	1.3(3)	10.7(10)	0.89(9)
		6_2^+	771.8(2)	2.5(25)	19.6(16)	0.45(5)

TABLE I. *(Continued).*

E_x (keV)	I_i^π	I_f^π	E_γ(keV)	I_γ	B.R.	R_{DCO}
		5^-	790.6(2)	1.2(3)	9.6(12)	1.23(15)
		6^+	1378.6(2)	2.7(7)	21.6(18)	0.51(10)
3622.3(1)	8_2^+	8^+	379.7(2)	1.6(4)	7.4(4)	0.76(17)
		6_2^+	786.2(1)	15.5(20)	71.6(10)	0.97(7)
		6^+	1392.7(2)	4.5(6)	21.0(10)	0.87(9)
3685.8(2)	(8_3^+)	8^+	443.2(1)	2.8(4)	74.4(46)	1.04(11)
		6^+	1456.2(3)	1.0(3)	25.6(46)	1.01(23)
4033.2(2)	8^-	7^-	507.9(3)	0.7(2)	7.7(8)	
		6_2^-	693.9(1)	8.5(18)	92.3(8)	1.02(4)
4142.5(2)	8_2^-	7_3^-	534.7(2)	1.0(3)	15(5)	
		7_2^-	577.0(2)	1.2(3)	19(6)	
		7^-	617.1(4)	0.3(1)	5(3)	
		6^-	1056.3(1)	3.9(9)	61(7)	0.89(16)
4350.3(2)	10^+	8^+	1107.9(1)	15.7(17)	100	1.11(5)
4366.2(2)	9^-	7_3^-	758.3(1)	5.6(4)	48.2(16)	0.96(6)
		7_2^-	800.5(2)	1.6(2)	14.1(12)	0.96(12)
		7^-	840.8(1)	4.4(4)	37.7(16)	0.96(6)
4423.3(2)	10_2^+	8_2^+	801.0(1)	19.2(23)	86.5(16)	0.93(6)
		8^+	1180.8(2)	3.0(4)	13.5(16)	1.00(4)
4472.7(2)	9_2^-	7_2^-	907.0(1)	3.2(4)	30.3(24)	1.19(16)
		7^-	947.2(2)	2.3(2)	21.3(20)	0.92(15)
		8^+	1230.3(2)	5.2(4)	48.5(26)	0.59(13)
4491.6(3)	9^+	7^+	1015.5(3)	2.1(4)	100	0.89(9)
4637.2(3)	(10_3^+)	10_2^+	213.5(3)	0.3(1)	5.1(6)	
		10^+	287.0(2)	1.1(2)	17.2(10)	1.06(14)
		(8_3^+)	951.2(2)	2.9(3)	44.9(20)	0.71(6)
		8^+	1394.7(3)	2.1(3)	32.8(20)	1.10(11)
4909.1(2)	10^-	8^-	875.9(1)	8.9(16)	100	1.03(4)
5237.3(4)	10_2^-	8_2^-	1094.8(3)	0.4(1)	100	0.99(17)
5307.5(2)	11^-	9^-	941.3(1)	9.1(7)	100	1.05(8)
5426.3(3)	12^+	10_2^+	1003.1(2)	20.3(4)	100	1.06(9)
5468(1)		10_2^+	1045(1)	4.2(18)	100	<0.25
5478.9(3)	(11_2^-)	9_2^-	1006.2(3)	7.2(5)	62(5)	0.88(9)
		10^+	1128.8(3)	4.5(3)	38(5)	0.99(14)
5569.0(3)	12_2^+	10^+	1218.7(3)	4.8(4)	100	1.06(11)
5738.1(5)	(12_3^+)	(10_3^+)	1100.9(4)	3.9(5)	100	0.63(24)
5913.6(4)	12^-	10^-	1004.5(3)	7.4(9)	100	1.00(7)
6366.5(3)	13^-	11^-	1059.0(2)	8.3(5)	100	1.09(7)
6449(1)		12^+	1023(1)	4.0(15)	100	<0.41
6542.8(4)	14^+	12^+	1116.5(3)	17.2(15)	100	1.06(13)
6564.6(4)	(13_2^-)	(11_2^-)	1085.7(3)	6.0(7)	100	1.55(3)
6937.0(4)	(14_2^+)	12_2^+	1368.0(3)	2.9(2)	100	
7066.2(5)	14^-	12^-	1152.6(3)	3.8(4)	100	1.09(15)
7534(1)		14^+	991(1)	4.7(12)	100	<0.27
7544.8(4)	15^-	13^-	1178.3(3)	4.5(10)	100	0.96(7)
7788.0(5)	(15_2^-)	(13_2^-)	1223.4(3)	2.8(3)	100	0.91(12)
7811.2(5)	16^+	14^+	1268.4(4)	7.1(5)	100	1.03(8)
8377.3(6)	16^-	14^-	1311.1(4)	2.7(4)	100	1.10(7)
8434.6(5)	(16_2^+)	(14_2^+)	1497.6(3)	2.0(10)	100	0.78(11)
8841.3(6)	17^-	15^-	1296.5(5)	3.8(10)	100	1.01(5)
9167.2(6)	(17_2^-)	(15_2^-)	1379.2(4)	2.0(10)	100	
9236.9(6)	18^+	16^+	1425.7(4)	5.0(15)	100	0.97(6)
9842(1)	(18^-)	16^-	1465(1)	1.7(7)	100	
10258.1(7)	(19^-)	17^-	1416.8(5)	3.4(9)	100	
10709(1)	(19_2^-)	(17_2^-)	1542(1)	2.0(10)	100	
10871.5(7)	(20^+)	18^+	1634.6(5)	1.9(9)	100	
11379(1)	(20^-)	(18^-)	1537(1)	1.0(6)	100	
11797.7(8)	(21^-)	(19^-)	1539.6(5)	2.5(9)	100	
13005(2)	(22^-)	(20^-)	1626(1)	0.8(4)	100	
13489(1)	(23^-)	(21^-)	1691(1)	1.8(8)	100	

A. Positive-parity bands

The results for the two major even-spin positive-parity bands (labeled 2 and 3 in Fig. 1) agree with earlier work [12–14]. A previously unreported $4_2^+ \rightarrow 2^+$ transition has been observed, but no evidence was seen for a corresponding $6_2^+ \rightarrow 4^+$ decay to complete the pattern. The present DCO ratios provide firm spin assignments for all but the 6937, 8435, and 10872 keV levels.

A new 9^+ state was added to band 1, and three additional decay branches with energies of 360, 530, and 1197 keV were seen from levels in this band to the even-spin states. The spins and parities of the three lowest states were previously assigned [10], and the DCO ratio of the 1016 keV decay supports the 9^+ assignment to the new level.

Four new decay branches with energies of 214, 287, 1395, and 1456 keV were observed from the 3686 and 4637 keV states, confirming a previously reported placement [10,13] for this likely third even-spin band (No. 4 in Fig. 1). Spins of (8), (10), and (12) $\hbar$ have been suggested for these states. The present DCO ratios generally support these assignments, as do the new decay branches. However, parentheses have been left on the spin suggestions due to the relatively large uncertainties on the DCO ratios for these weak lines. Positive parity is strongly suggested since all the decay branches are to positive-parity states and it is extremely unlikely that the 1395 and 1456 keV decays would have $M2$ character.

New lines at 991, 1023, and 1045 keV were clearly seen in coincidence with a number of transitions in band 2, as shown in Fig. 2. The coincidence relations show that they feed into the band as indicated in the upper left portion of Fig. 1 above band 1. No evidence could be found for decays between these new states nor to other levels, such as the 9^+ state. These levels were drawn above the odd-spin band in Fig. 1 merely because space was available there. The low DCO ratios of these decays would be consistent with spin assignments of 11^+, 13^+, and 15^+, but other spins, such as 9^+, 11^+, and 13^+, are also possible.

B. Negative-parity bands

Although it is weakly populated, evidence has been seen for the 3^- state at 2402 keV. This state had been previously reported [6,10], but has been omitted from more recent level schemes. The new transitions observed to the 3^- state from the two 4^- levels confirm its placement in the level scheme. The spin and parity of the 5^- state at 2817 keV were assigned [10] on the basis of angular distribution and linear polarization measurements of the 1489 keV transition. Four levels were assigned a spin of $7\hbar$ with varying degrees of confidence in Ref. [10], in addition to the 7^+ state discussed previously, and this interpretation has been followed in the more recent level schemes [12–14]. The present work confirms the spin assignment and placement of three of these, but indicates a different ordering of the transitions in one band, as discussed below, and hence does not support a fourth 7^- state at 3511.3 keV. New transitions have been observed between each of the three confirmed (as discussed below) 7^- states at 3525, 3566, and 3608 keV and the 5^- level at 2817 keV. This is one of several indications of strong mixing between the low-lying negative-parity states. The 9^- state at 4366 keV decays to all three 7^- states and was placed in the level scheme so that decay sequence 5 would represent the negative-parity yrast sequence. There is no evidence for mixing above the 9^- state in the decay sequence, and the measured DCO ratios provide firm spin assignments from the 7^- state at 3525 keV through the 17^- level.

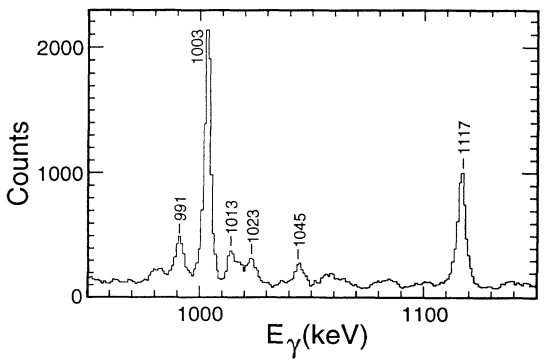

FIG. 2. The sum of γ spectra in coincidence with the 786 and 801 keV transitions in band 2.

A new (5^-) state was located at 3073 keV. It is firmly placed in the level scheme by seven transitions linking it to previously known states. The DCO ratios which could be measured are consistent with this tentative spin-parity assignment, but the state is too weakly populated to allow a firm assignment. As mentioned before, the negative-parity states in this energy range are so strongly mixed that assignments to individual bands are not very meaningful. For the purpose of drawing a level scheme, this second state of odd spin has been grouped with the other yrare odd-spin states in band 6 discussed below. The DCO ratio of the 801 keV decay from the 4366 keV 9^- state to the 3566 keV level provides a spin-parity assignment of 7^- to the latter level.

A decay sequence including the 1005.6, 1085.4, and 1222.6 keV transitions was reported decaying into the yrast 8^+ state in Refs. [12,13]. The same decay sequence has been seen in the present work, but with an intervening 1230 keV γ ray between the new 4473 keV level and the 8^+ state. Two more decay branches at 907 and 947 keV were observed from the 4473 keV level to 7^- states. Another decay branch at 1129 keV was also seen from the 5479 keV level to the yrast 10^+ state. These additional decays, which can be seen in Fig. 3, confirm the present placement of the band (No. 6 in Fig. 1). The DCO ratios for the decays of the 4473 keV level to the two 7^- states imply $E2$ transitions and, hence, an assignment of 9^-. The DCO ratio of the 1230 keV decay transition to the 8^+ level is consistent with $E1$ decay. The spins of the higher members of this band have been placed in parentheses since the DCO ratios for these weaker γ rays are not as decisive.

Another (5^-) state has been found at 3142 keV. It is fed by a 465 keV decay from the 7_3^- level and decays by an 1813 keV transition to the 4^+ yrast level. The spin

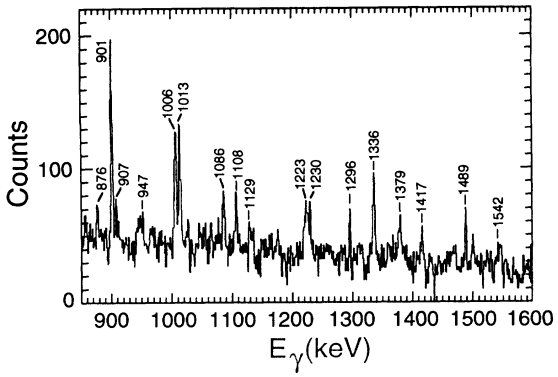

FIG. 3. The sum of γ spectra in coincidence with the 907, 1086, 1223, and 1230 keV transitions in band 6.

and parity of the previously known 7_3^- level above it are determined by the DCO ratio of the 758 keV decay from the 4366 keV 9^- state. No further members of this decay sequence (No. 7 in Fig. 1) could be found.

The 1489, 522, 694, 876 keV decay sequence (No. 8 in Fig. 1) has been known for some time, but the ordering of the transitions within the sequence has varied. (A second 522 keV transition from the 7_3^- to the 6^- level is also known, but it has different coincidence relations and does not affect the present discussion.) The 522 keV γ ray was placed directly above the 1489 keV decay and no other members of the sequence were reported in Refs. [7,8]. The 522 keV transition was moved up one step in Ref. [9] and another two steps higher in Ref. [10]. It was then lowered by one step in Refs. [12–14] and recently lowered again to just above the 1489 keV transition in the g-factor study [11] which populated only lower-lying states. Only in Ref. [10] were any other decay branches reported in support of the proposed level ordering. However, we have not been able to confirm these additional decay branches at 269.0, 403.9, 423.5, and 1144.2 keV. There is no evidence of an 1144 keV line in our 1005 keV gate, a 269 keV line in the 876 keV gate, or an 876 keV line in the 269 keV gate. Moreover, the 404, 423, and 875 keV γ rays were later shown [17] to form a decay sequence in ^{83}Sr.

We have found clear evidence to place the 522 keV decay between the 1489 and 694 keV transitions, the same position reported in Refs. [7,8,11]. In addition to the intensity balance, our placement is based on new decay branches at 266, 333, 508, 814, and 1110 keV from levels in this band. The 333 keV decay leads to a new 4^- state at 3007 keV, which decays by a 605 keV γ ray to the 3^- level and by 1011, 1318, and 1678 keV transitions to positive-parity states. Most of these new decays can be seen in the spectrum in coincidence with the 694 keV transition shown in Fig. 4. In particular, the 814 keV branch proceeds to the previously established 5^+ state, many of whose decay lines can also be seen in the spectrum (513, 837, and 1115 keV).

The DCO ratios of the 1318 and 1678 keV lines are consistent with $E1$ decay as is the 814 keV branch from the 3339 keV state above, while that of the 333 keV transition implies $E2$ decay. The small DCO ratio of the 522 keV transition is consistent with the large negative a_2 angular distribution coefficient measured in Ref. [10] and implies a mixed $E2/M1$ decay with a considerable $E2$ component. These considerations provide the spin-parity assignments for the 4^- and 6^- states, and the DCO ratios of the higher transitions imply an $E2$ cascade up through the 8377 keV 16^- state.

The spins and parities of the yrast 4^- and 6^- levels at 2824 and 3086 keV, respectively, were assigned in Refs. [9,10], and the present DCO ratios are consistent with these assignments. Two more states have been found in this band (No. 9 in Fig. 1) with spins and parities of 8^- and 10^-. The former decays by an $E2$ transition to the 6^- level and to all three 7^- states, while only the in-band $E2$ decay has been seen from the latter. The placement of the even-spin states in decay sequences is clear, since there are no decays between the sequences, even though the lowest 8^- state decays to the higher-lying 6^- and 4^- levels and the higher 8^- state decays to the lowest 6^- and 4^- levels.

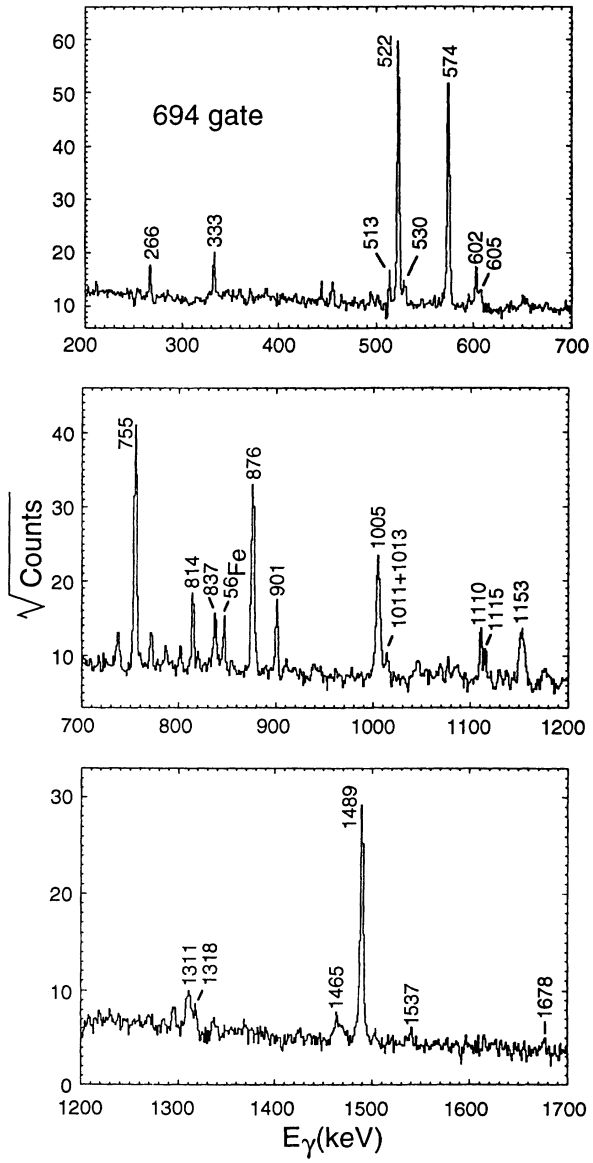

FIG. 4. The spectrum of γ rays in coincidence with the 694 keV transition in band 8. The square root of the number of counts is graphed to display a wider dynamic range.

IV. MEAN LIFETIMES AND TRANSITION STRENGTHS

A. Lifetimes and side-feeding times

The lifetimes of 22 levels in four bands were determined using the Doppler-shift attenuation method (DSAM). The line shapes in the 30° coincidence spectra were analyzed using a computer code [3] which simulates the slowing down and decay process. The simulation takes into account such effects as the deceleration of the beam in the target before interaction, the distribution of recoil velocities, the detector resolution and geometry, direct feeding from higher-lying states, and continuum side feeding. The electronic stopping powers were taken from the compilation of Northcliffe and Schilling [18] and scaled by a few percent to the experimental α stopping powers [19] in Fe. They are generally within 10% of the values suggested in Ref. [20]. The nuclear component of the stopping powers was calculated using the Bohr ansatz [21,22], and the angular straggling due to atomic collisions was treated in Blaugrund's approximation [23]. Although the target was infinitely thick to the beam, the cross section for producing ^{82}Sr drops to zero at about 75 MeV because of the entrance Coulomb barrier. Therefore, the range of initial recoil velocities, which were accounted for in the simulation, extended from 2.5% to 2.9% of the speed of light.

The 30° line shapes were determined from spectra in coincidence with one or more transitions above or below the line of interest. The highest transition in each cascade whose line shape could be determined was first fitted assuming no direct or side feeding. This effective lifetime is only an upper limit for that state, but provides a feeding correction for the levels below. The lifetimes, side-feeding times and relative intensities of all levels above the one of interest were included in each line shape simulation. Where the statistical accuracy was adequate, the lifetime was determined by fitting the line shape gated from the transition above to eliminate the effect of side feeding into the state under study. In these cases the line shape gated by the transition below was then fitted by holding the lifetime constant at the previously determined value and varying the side-feeding time. This procedure provided a direct determination of the side-feeding time for use in fitting the lower transitions. In the other cases side-feeding times were approximated by interpolating and extrapolating the measured values.

The goodness of fit χ^2 per degree of freedom (χ^2_ν) between the best simulations and the measured line shapes was generally around 1. To estimate the uncertainties, the lifetime or side-feeding time was then varied above and below the best-fit value until χ^2_ν increased by 1. This roughly corresponds to the 1% confidence limit [24] and may be a somewhat conservative estimate of the statistical uncertainties. However, it is probably a reasonable estimate of the total uncertainties, including in some way contributions from uncertainties in the stopping powers, unresolved contaminant lines, etc. Examples of the line shapes are shown in Figs. 5 and 6, along with the best fits and the $\chi^2_{\nu,\min}+1$ fits. A comparison of line shapes gated from above and below can be seen for the 1116.5 keV line in Fig. 5. The side-feeding times determined by such fits are graphed in Fig. 7 as a function of excitation energy. This graph may oversimplify the situation since side-feeding times depend on many other factors, but it shows a clear trend represented by the dashed line, which is at least consistent within the uncertainties and provides some justification for the extrapolations. The trend is similar to that reported for ^{79}Rb [25] in the ^{63}Cu(^{19}F,2pn) reaction at 65 MeV, but the present side-feeding times are a factor of 2 or 3 longer, perhaps reflecting the different reactions or the fact that the present measurements extend to higher excitation energies. Cristancho *et al.* [26] have examined side-feeding times both experimentally and theoretically. They find that side-feeding times vary exponentially with spin for the yrast bands, in agreement with the trend in Fig. 7. The magnitudes appear to vary from reaction to reaction.

The results of the present DSAM lifetime fits are listed

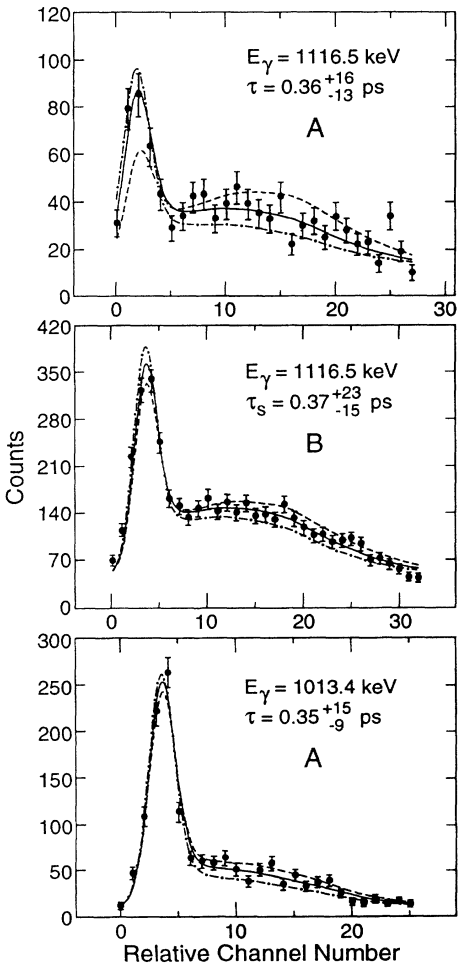

FIG. 5. 30° coincidence spectra of the 1116.5 keV $14^+ \rightarrow 12^+$ and 1013.4 keV $8^+ \rightarrow 6^+$ transitions. The letters "*A*" and "*B*" indicate whether the gating transitions were above or below the decay of interest. The dispersion is 0.8 keV/channel. The solid lines indicate the best DSAM simulation fits, while the broken lines correspond to simulations for the indicated error limits.

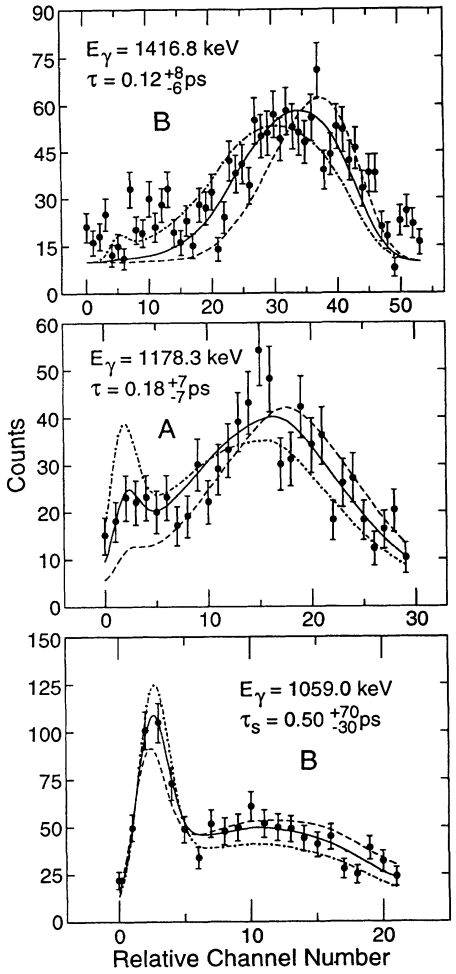

FIG. 6. 30° coincidence spectra of the 1416.8 keV $(19^-) \rightarrow 17^-$, 1178.3 keV $15^- \rightarrow 13^-$, and 1059.0 keV $13^- \rightarrow 11^-$ transitions. Refer to the caption of Fig. 5 for more information.

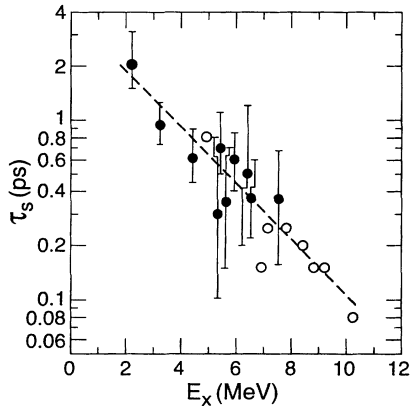

FIG. 7. Side-feeding times as a function of excitation energy. The points represented by solid circles were determined by a comparison of DSAM fits to line shapes gated by transitions above and below the one of interest, while the open circles represent the extrapolated values used in the analysis of the lines which could be gated only from below. The straight line is drawn to guide the eye.

in Table II along with some previous recoil-distance measurements [9] (RDM) for the lower-lying states. There is a significant difference in the only lifetime measured by both methods, that of the 2229 keV 6^+ state. However, it is not clear if the RDM value was corrected for feeding since it was the highest one measured in the band, and the $E2$ strength based on the present measurement is in better agreement with those of the other transitions in the band.

B. Transition strengths

The transition strengths $B(E2)$ and transition quadrupole moments Q_t for the $\Delta I = 2$ decays within each band are also listed in Table II. The Q_t values, which are calculated from the rotational formula

$$Q_t^2 = \frac{16\pi}{5} \langle I\ K\ 2\ 0 \mid I-2\ K\rangle^{-2} \times B(E2, I \rightarrow I-2) \ , \quad (2)$$

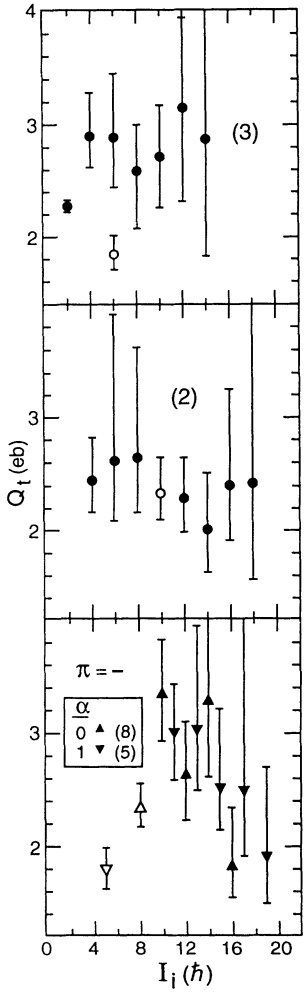

FIG. 8. The transition quadrupole moments Q_t inferred from the lifetimes determined in the present DSAM experiment and from an earlier RDM measurement [9]. The points represented by open symbols may not have been corrected for feeding. The numbers in parentheses identify the bands with those shown in Fig. 1.

depend somewhat on the intrinsic angular momentum K assumed for each band. A value of $K = 0$ was used for the GSB (band 3) and $K = 2$ was used for band 2, although $K = 0$ cannot be completely ruled out since another 0^+ state is known [6] at 1.31 MeV. The low-lying negative-parity states are strongly mixed. We have used $K = 3$ for the two negative-parity bands (No. 5 and 8), under the assumption that they are signature partners, since $E2$ decays can be followed down to the 3^- and 4^- states. The transition quadrupole moments are displayed graphically in Fig. 8. As mentioned before, the RDM lifetimes reported in Ref. [9] for the highest measured states in each band may not have been corrected for feeding and appear to be anomalously long in some cases. The Q_t values based on these lifetimes are shown as open symbols in Fig. 8. Except for these points, the transition quadrupole moments inferred from the RDM and DSAM lifetime measurements appear to be consistent.

The transition quadrupole moments provide a measure of the nuclear quadrupole deformation β_2. If the nucleus is axially symmetric the deformation is given approximately by

$$\beta_2 = \sqrt{\frac{49\pi}{80} + \frac{7\pi Q_t}{6eZr_0^2A^{2/3}}} - \sqrt{\frac{49\pi}{80}}. \quad (3)$$

For purposes of discussion, some β_2 values have been inferred from the transition quadrupole moments using $r_0 = 1.2$ fm.

A number of $\Delta I = 1$ and 2 transitions were previously known from the excited 2^+ band to the GSB and several new decays were added in the present work. To better

TABLE II. Mean lifetimes of states in ^{82}Sr measured by the Doppler-shift attenuation method, along with previous recoil-distance measurements [9], side-feeding times τ_S, intraband transition strengths $B(E2)$, and transition quadrupole moments Q_t.

E_x (keV)	I_i^π	E_γ (keV)	τ (ps)	τ_S (ps)	$B(E2)$ (W.u.)[a]	Q_t (e b)
573.5	2^+	573.5	12.80(50) [b]		48(2)	2.27(5)
1328.4	4^+	754.9	1.40(30) [b]		112^{+31}_{-20}	2.89^{+37}_{-27}
2229.2	6^+	900.8	0.53^{+21}_{-16} [c]	2.05^{+105}_{-55}	123^{+53}_{-35}	2.88^{+57}_{-44}
3242.6	8^+	1013.4	0.35^{+15}_{-9}	0.95^{+32}_{-22}	103^{+36}_{-31}	2.58^{+41}_{-42}
4350.3	10^+	1107.9	0.20^{+9}_{-6}	0.62^{+28}_{-17}	116^{+50}_{-36}	2.70^{+53}_{-46}
5569.0	12_2^+	1218.7	0.09^{+8}_{-8}	0.35^{+35}_{-20}	159^{+1274}_{-75}	3.14^{+630}_{-85}
6937.0	(14_2^+)	1368.0	0.06^{+9}_{-5}	0.15 [d]	134^{+671}_{-80}	2.86^{+420}_{-110}
8434.6	(16_2^+)	1497.6	<0.26 [e]	0	> 20	>1.09
1995.9	4_2^+	820.3	1.90(50) [b]		33^{+12}_{-7}	2.43^{+40}_{-27}
2836.1	6_2^+	840.2	0.90(50) [b]		75^{+94}_{-27}	2.61^{+130}_{-52}
3622.3	8_2^+	786.2	1.00(50) [b]		92^{+92}_{-31}	2.63^{+110}_{-48}
4423.3	10_2^+	801.0	1.30(30) [b]		78^{+23}_{-15}	2.32^{+32}_{-23}
5426.3	12^+	1003.1	0.48^{+16}_{-12}	0.70^{+40}_{-20}	79^{+26}_{-20}	2.28^{+35}_{-31}
6542.8	14^+	1116.5	0.36^{+16}_{-13}	0.37^{+23}_{-15}	62^{+35}_{-19}	1.99^{+50}_{-33}
7811.2	16^+	1268.4	0.13^{+7}_{-6}	0.25 [d]	91^{+78}_{-32}	2.38^{+86}_{-46}
9236.9	18^+	1425.7	0.07^{+10}_{-6}	0.15 [d]	94^{+560}_{-55}	2.40^{+400}_{-86}
10871.5	(20^+)	1634.6	<0.3 [e]	0	> 11	>0.82
4033.2	8^-	693.9	3.80(60) [b]		58^{+11}_{-8}	2.32^{+21}_{-16}
4909.1	10^-	875.9	0.52^{+16}_{-12}	0.80 [d]	144^{+43}_{-34}	3.34^{+47}_{-42}
5913.6	12^-	1004.5	0.39^{+16}_{-11}	0.60^{+25}_{-20}	97^{+38}_{-28}	2.62^{+47}_{-41}
7066.2	14^-	1152.6	0.12^{+7}_{-6}	0.25 [d]	159^{+158}_{-58}	3.27^{+140}_{-67}
8377.3	16^-	1311.1	0.20^{+8}_{-8}	0.20 [d]	50^{+33}_{+14}	1.80^{+52}_{-28}
9842	(18^-)	1465	<0.27 [e]	0	> 21	>1.17
2817.2	5^-	415.6	4.40(80) [b f]		13^{+3}_{-2}	1.79^{+19}_{-14}
5307.5	11^-	941.3	0.43^{+15}_{-10}	0.30^{+50}_{-30}	122^{+37}_{-31}	3.00^{+42}_{-42}
6366.5	13^-	1059.0	0.22^{+11}_{-9}	0.50^{+70}_{-30}	132^{+91}_{-44}	3.02^{+91}_{-55}
7544.8	15^-	1178.3	0.18^{+7}_{-7}	0.35^{+35}_{-20}	95^{+60}_{-26}	2.50^{+70}_{-38}
8841.3	17^-	1296.5	0.11^{+8}_{-8}	0.15 [d]	96^{+255}_{-40}	2.48^{+230}_{-59}
10258.1	(19^-)	1416.8	0.12^{+8}_{-6}	0.08 [d]	57^{+56}_{-23}	1.89^{+78}_{-43}
11797.7	(21^-)	1539.6	<0.08 [e]	0	>56	>1.86

[a] 1 W.u. = 21.2 e^2 fm^4.
[b] Recoil-distance measurement from Ref. [9].
[c] Value reported in Ref. [9] is 1.3(2) ps.
[d] Extrapolated value.
[e] Effective lifetime not corrected for direct or side feeding.
[f] Measured from the 1488.8 keV transition.

TABLE III. Interband transition strengths $B(M1)$ and $B(E2)$ based on the lifetimes reported in Ref. [9] and the present branching ratios. A mixing ratio of $\delta = 0.25$ was used to calculate the $B(M1)$ values, as discussed in the text.

E_x (keV)	I_i^π	E_γ	I_f^π	$B(E2)$(W.u.)	E_γ	I_f^π	$B(M1)$ (W.u.)
1175.6	2_2^+	1175.7	0^+	0.3(1)	602.0	2^+	0.010(4)
1995.9	4_2^+	1422.4	2^+	0.05(2)	667.5	4^+	0.020(5)
2836.1	6_2^+				606.9	6^+	0.040(22)
3622.3	8_2^+	1392.7	6^+	1.5(10)	379.7	8^+	0.040(25)
4423.3	10_2^+	1180.8	8^+	1.7(4)			

assess the degree of mixing between these two bands, the $B(M1)$ and $B(E2)$ transition strengths have been listed in Table III for the $\Delta I = 1$ and 2 decays, respectively. The DCO ratios determined for the $\Delta I = 1$ transitions in the present work are consistent with the mixing ratio values of $|\delta| = 0.18(32)$ and 0.28(69) reported in Ref. [10] for the 606.7 and 667.5 keV transitions, respectively. We have used a constant value of $|\delta| = 0.25$ to determine the $B(M1)$ values for the $\Delta I = 1$ transitions, but $B(M1)$ is not very sensitive to δ as long as it is small. The $B(E2)$ values for the $\Delta I = 1$ decays are much more sensitive to δ and have not been included in Table III, since the mixing ratios are not known with sufficient accuracy.

V. DISCUSSION

The ^{82}Sr level scheme in Fig. 1 presents a rich band structure. Four positive-parity bands are known and an excited band becomes yrast at spin $12\hbar$. The low-lying negative-parity states are strongly mixed and four rotational bands form above them. Both known 9^- states decay with comparable branches to three nearly degenerate 7^- states, each of which in turn decays to two 5^- levels, and the lowest 4^- and 6^+ states. The closest analogy is to the structure of the isotone ^{80}Kr [27,28], which exhibits a relatively similar positive-parity band structure and has two 9^- and three 7^- states which are nearly degenerate and strongly mixed. There are also similarities with the heavier isotone ^{84}Zr [29,30] although not as many bands are known at present and there is no evidence for multiple negative-parity structures.

The average transition quadrupole moment $\overline{Q_t}$ of 2.8(2) eb in the GSB of ^{82}Sr would correspond to an axial quadrupole deformation of $\beta_2 = 0.33$. The comparison of $\overline{Q_t}$ values among the nearby isotopes and isotones in Fig. 9 shows that the deformation of ^{82}Sr forms a local maximum, comparable only to that of ^{80}Sr. The peak at $Z = 38$ among the $N = 44$ isotones is consistent with the general systematics [37] of maximum deformation at midshell ($N, Z \approx 39$), as is the general decrease of $\overline{Q_t}$ with increasing N for the $Z = 38$ isotopes. However, the local maximum in deformation for ^{82}Sr violates the latter trend and shows the importance of nuclear structure effects.

A. Band mixing

With the additional branches observed in the present work, eight decays are known from bands 2 to 3. The question of whether these interband transitions represent strong mixing between bands 2 and 3 or just occur because the decay energies are favorable can be answered directly, since many of the lifetimes are known. Table III shows that the interband transition strengths are quite weak. The $E2$ strengths are about two orders of magnitude less than those of the intraband decays in each of the bands, and the $M1$ strengths are more than an order of magnitude below typical values between signature-partner bands in odd-A nuclei. Thus there is little mixing between bands 2 and 3 in spite of the prevalence of interband decays. Band mixing calculations show that the interband $E2$ strengths are roughly consistent with an interaction matrix element of 50–100 keV.

Some decays are also known from band 1 to bands 2 and 3. Although lifetimes are not known in this weakly populated band, the interband transition strengths can be estimated by assuming that the intraband 837 keV decay has the same strength as the corresponding 840 keV decay in band 2. This would imply an $M1$ strength of 0.023 Weisskopf units (W.u.) for the decay of the 5^+ state to the 4_2^+ state in band 2 and 0.002 W.u. for the decay to the 4^+ state in band 3. Thus the band 1 to 2 branch is as weak as those from band 2 to 3, while the band 1 to 3 decay is yet another order of magnitude weaker.

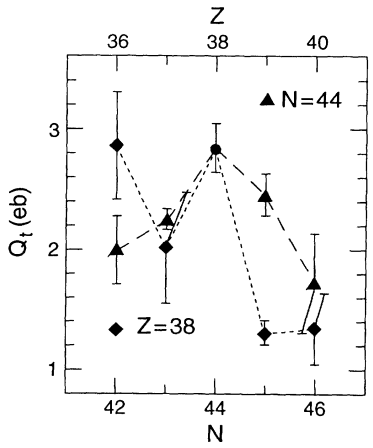

FIG. 9. The average GSB transition quadrupole moments Q_t of the nearby isotopes and isotones of $^{82}_{38}Sr_{44}$. The standard deviations of the values are shown as error bars. The neutron number N is indicated along the bottom for the $Z = 38$ isotopes ^{80}Sr [31], ^{81}Sr [3], ^{83}Sr [32,33], and ^{84}Sr [34], and the proton number Z is shown along the top for the $N = 44$ isotones ^{80}Kr [27], ^{81}Rb [35], ^{83}Y [36], and ^{84}Zr [29].

The situation is different among the low-lying negative-parity states. Although few lifetimes are known among these states, the nearly equal branching ratios with nearly equal decay energies imply nearly equal transition strengths between the multiplets of states and hence maximal mixing. Many of these states also decay to the positive-parity levels. Although these parity-changing decays are energetically favored, they still suggest that some of the intraband transitions are weaker than in the positive-parity bands or higher in the negative-parity bands. Where lifetimes are available, the 694 keV $8^- \rightarrow 6_2^-$ transition strength is somewhat weaker than higher ones in the band and that of the 416 keV $5^- \rightarrow 3^-$ decay is much weaker (13 W.u.). Above a spin of about $9\hbar$ the decays out of the bands become too weak to observe and the intraband $E2$ strengths become quite enhanced. There is a considerable variation in the spacings of the multiplets which cannot be reproduced by a simple two- or three-level band mixing calculation with a constant interaction strength. A more fundamental theoretical calculation would be required to account for the level spacings and changes in collectivity.

B. Cranked shell-model analysis

The transition strengths measured in bands 2, 3, 5, and 8 are strongly enhanced and support their interpretation as rotational bands. Although lifetimes are not known in the other decay sequences, numbers 1 and 6 appear to be good candidates for rotational bands. Not enough transitions are known in the other cascades to be useful in the analysis. The band structure is less clear for the low-lying negative-parity states, as discussed above. We have calculated the kinematic moments of inertia $J^{(1)}$ in these six bands as they are grouped in Fig. 1. They are graphed as a function of rotational frequency ω in Fig. 10 along with the dynamic moments of inertia $J^{(2)}$ for the negative-parity bands. The intrinsic spins K assumed for each band are shown in the figure.

1. Positive-parity bands

The kinematic moments of inertia in the positive-parity bands start from rather low values and increase to the rigid-body value at high spins as is typical for even-even nuclei [38]. The rise is smooth in the case of the GSB and quite sharp in band 2, but they converge to the same value at 0.9 MeV/$\hbar$. The three points known for band 1 appear to follow those of the GSB more closely than band 2, which might be expected to be its signature partner.

Increases in $J^{(1)}$, especially smooth ones, are sometimes interpreted as changes in the deformation or collectivity. However, $J^{(1)}$ increases by a factor of 4 in the GSB while the transition quadrupole moments remain rather constant at an average value of 2.8(2) eb. The first Q_t value is 20% lower than the average, but this is no factor of 4, and there is no evidence of further increase for higher spins. Likewise, the moments of inertia in band 2 increase rapidly by a factor of 2.7 while the Q_t values remain remarkably constant, averaging 2.4(2) eb.

The lifetime measurements also shed light on the crossing between bands 2 and 3. At low spins band 2 lies 600 keV above band 3 (GSB), but this difference decreases and band 2 becomes yrast at the 12^+ state. Clearly, band 2 has a higher moment of inertia over this range, as deduced from the energy spacings and shown in Fig. 10. This is often interpreted to mean that bands such as No. 2 are more deformed. Quite surprisingly, the average Q_t value of 2.4(2) eb in band 2, which would correspond to an axial deformation of $\beta_2 = 0.28$, is smaller than the average of 2.8(2) eb in band 3 ($\beta_2 = 0.33$).

The dynamic moments of inertia $J^{(2)}$ in the GSB of ^{80}Sr and ^{82}Sr were compared in Ref. [13]. Both curves show moderate peaks at $\hbar\omega = 0.56$ and 0.75 MeV, which were interpreted as $\pi g_{9/2}$ and $\nu g_{9/2}$ alignments, respectively. The measured [11] g factor of +0.7(1) for the 8^+ state supports the interpretation of a gradual proton alignment under way at this spin. The Hartree-Fock-Bogolyubov cranking (HFBC) calculations [4,13] predict

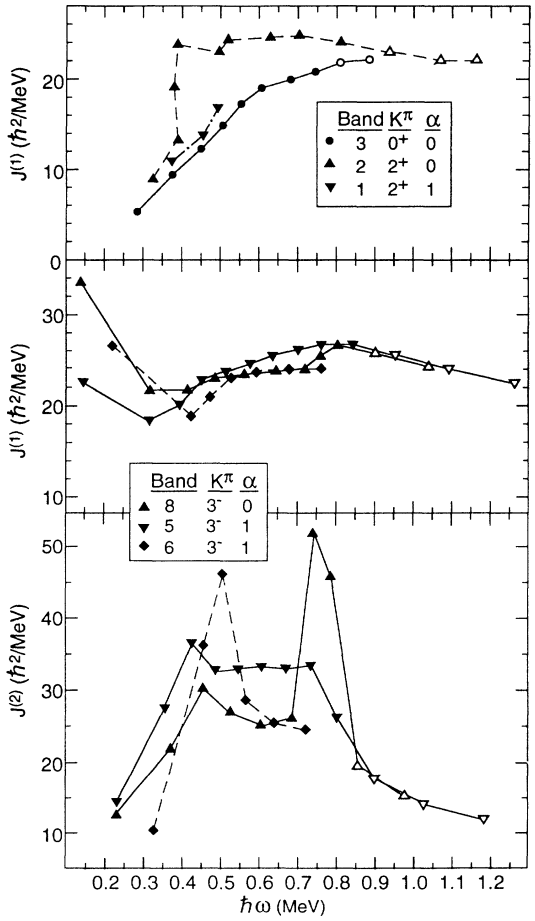

FIG. 10. The kinematic and dynamic moments of inertia $J^{(1)}$ and $J^{(2)}$ for bands in ^{82}Sr. The legends identify the bands according to the numbers in Fig. 1 and indicate the K values used in the analysis. The open symbols represent previously published transitions [12,13] which were not observed in the present experiment.

a well-deformed nearly prolate shape with $\beta_2 = 0.34$ for the low-spin portion of the GSB of ^{82}Sr. This is in excellent agreement with the average Q_t value of 2.8(2) e b measured for this band. However, there is no indication in Fig. 8 for a change toward a less deformed oblate shape ($\beta_2 = 0.22, \gamma = -50°$) at higher spins unless this occurs above the 14^+ state.

A less deformed oblate minimum in the HFBC calculations was identified in Refs. [4,13] with the low-spin portion of band 2. The measured Q_t values for this band do imply a somewhat lower axial deformation of $\beta_2 = 0.28$, but remain more constant than appears to be predicted.

2. *Negative-parity bands*

The kinematic moments of inertia in the negative-parity bands are quite similar and do not vary as much with frequency. The $J^{(1)}$ values are somewhat higher at the lowest spins, but this is the region where the band structure is less clear because the states are so strongly mixed. The more constant behavior of the moments of inertia (compared to the positive-parity bands) is typical [38] of bands with one or more quasiparticles.

Two-quasiproton configurations have been suggested [13] for the low-lying portions of bands 5 and 8. There are peaks in the dynamic moments of inertia for 0.4 MeV $< \hbar\omega <$ 0.5 MeV in all three negative-parity bands, some of which have been interpreted as $g_{9/2}$ neutron alignments. The distinct peak in $J^{(2)}$ for band 8 and the sharp descent in band 5 at $\hbar\omega \approx 0.75$ MeV have been interpreted [13] as the next proton quasiparticle alignment.

A triaxial shape with $\beta_2 = 0.28$ and $-30° < \gamma < -20°$ is predicted in the HFBC calculations for the negative-parity two-quasiproton configuration. This would correspond [39] to a transition quadrupole moment of $Q_t \approx 3$ e b in good agreement with the values measured for states with spins around 10^-. For higher spins, the measured Q_t values show a definite decreasing trend. This could possibly correspond to the predicted shape change from triaxial to oblate due to the $\nu g_{9/2}$ alignment.

VI. SUMMARY

High-spin states in ^{82}Sr were populated using the ^{56}Fe(^{29}Si,2pn) reaction at 95 MeV with a thick 78 mg/cm^2 natural Fe target. γ-γ coincidences were detected with three Compton-suppressed Ge detectors placed at 90° to the beam and two at 30°.

Nine new states and 38 new transitions were found. DCO ratios provided firm spin assignments to a number of states. These results have helped to clarify the band structure of ^{82}Sr. Some of the new transitions have provided a firm assignment for the placement of the 522 keV line, whose position has varied considerably in the literature. Other transitions have placed the yrare negative-parity band. The new negative-parity states and the transitions between them have shown a high degree of mixing among the states below 10^-.

Lifetimes or limits have been determined for 22 states using the DSAM, and a comparison of the line shapes in coincidence with transitions above and below has provided a direct determination of the continuum side-feeding times into 10 levels. These mean lifetimes, along with those of the lower states measured in an earlier RDM experiment [9], provide new insights into the shapes of four bands.

The average transition quadrupole moment of 2.8(2) e b in the GSB, which corresponds to an axial deformation of $\beta_2 = 0.33$, is similar to that of ^{80}Sr and larger than those of the other neighboring isotones and isotopes. This large deformation for a transitional nucleus is somewhat anomalous among the Sr isotopes, but is predicted by HFBC calculations. The kinematic moment of inertia in this band increases with spin by a factor of 4, but the Q_t values remain constant within the uncertainties.

Quite surprisingly, the transition quadrupole moment of the excited 2^+ band, which crosses the GSB to become yrast and has a larger moment of inertia, is lower [$\overline{Q_t} =$ 2.4(2) e b], corresponding to a less deformed shape with $\beta_2 = 0.28$ if axially symmetric. A number of $\Delta I = 1$ and 2 decay branches are seen between this band and the GSB, but their transition strengths are one to two orders of magnitude weaker than those of intraband transitions.

The Q_t values in the negative-parity bands are also large. The average of about 3 e b below spin $15\hbar$ is consistent with the predicted triaxial shape of $\beta_2 = 0.28$ and $-30° < \gamma < -20°$. The transition quadrupole moments decrease significantly at higher spins. Many of the negative-parity states below spin $10\hbar$ are strongly mixed. The decay branches between the two 9^-, three 7^-, and three 5^- levels are nearly equal.

This work was supported in part by the National Science Foundation.

[1] R. Bengtsson, P. Möller, J.R. Nix, and J. -y. Zhang, Phys. Scr. **29**, 402 (1984); P. Möller, J.R. Nix, W.D. Myers, and W.J. Swiatecki (unpublished).

[2] C.J. Lister, B.J. Varley, H.G. Price, and J.W. Olness, Phys. Rev. Lett. **49**, 308 (1982).

[3] E.F. Moore, P.D. Cottle, C.J. Gross, D.M. Headly, U.J. Hüttmeier, S.L. Tabor, and W. Nazarewicz, Phys. Rev. C **38**, 696 (1988).

[4] W. Nazarewicz, J. Dudek, R. Bengtsson, T. Bengtsson, and I. Ragnarsson, Nucl. Phys. **A435**, 397 (1985).

[5] E. Nolte, Y. Shida, W. Kutschera, R. Prestele, and H. Morinaga, Z. Phys. A **268**, 267 (1974).

[6] J.B. Ball, J.J. Pinajian, J.S. Larsen, and A.C. Rester, Phys. Rev. C **8**, 1438 (1973).

[7] T. Higo, S. Matsuki, and T. Yanabu, Nucl. Phys. **A393**, 224 (1983).

[8] C.A. Fields, F.W.N. de Boer, E. Sugarbaker, and P.M. Walker, Nucl. Phys. **A363**, 352 (1981).

[9] A. Dewald, Ph.D. Dissertation, University of Cologne, 1982; A. Dewald, U. Kaup, W. Gast, A. Gelberg, K.O. Zell, and P. von Brentano, in *Proceedings of the 4th International Conference on Nuclei Far from Stability,* Helsingør, Denmark, 1981, edited by P.G. Hansen and G.B. Nielsen (CERN, Geneva, 1981).

[10] P.S. Haskins, F.E. Dunnam, R.L. Coldwell, A.C. Rester, R.B. Piercey, M.L. Muga, H.A. Van Rinsvelt, R.W. Smart, H.J.M. Aarts, J.D. Fox, L.C. Dennis, and C.B. Saw, Phys. Rev. C **32**, 1897 (1985).
[11] A.I. Kucharska, J. Billowes, and C.J. Lister, J. Phys. G **15**, 1039 (1989).
[12] D.G. Sarantites, C. Baktash, N.G. Nicolis, G. Garcia-Bermudez, V. Abenante, J.R. Beene, N.R. Johnson, M.L. Halbert, D.C. Hensley, F.K. McGowan, H.C. Griffin, I.Y. Lee, Z. Majka, M.A. Riley, T.M. Semkow, D.W. Stracener, and A. Virtanen, Phys. Rev. Lett. **64**, 2129 (1990).
[13] C. Baktash, G. Garcia-Bermudez, D.G. Sarantites, W. Nazarewicz, V. Abenante, J.R. Beene, H.C. Griffin, M.L. Halbert, D.C. Hensley, N.R. Johnson, I.Y. Lee, F.K. McGowan, M.A. Riley, D.W. Stracener, T.M. Semkow, and A. Virtanen, Phys. Lett. B **255**, 174 (1991).
[14] S. Suematsu, S. Mitarai, J. Mukai, H. Tomura, A. Odahara, R. Nakatani, T. Kuroyanagi, S.E. Arnell, Ö. Skeppstedt, D. Jerrestam, J. Nyberg, A. Atac, H. Roth, N. Gjørup, J. Jongmann, and G. Sletten, Kyushu University Tandem Accelerator Laboratory Report, 1988-1990, p. 101.
[15] P.C. Womble, J. Döring, T. Glasmacher, J.W. Holcomb, G.D. Johns, T.D. Johnson, T.J. Petters, M.A. Riley, V.A. Wood, and S.L. Tabor, Phys. Rev. C **47**, 2546 (1993).
[16] E. F. Moore, Ph.D. Dissertation, Florida State University, 1988.
[17] J. Döring, L. Funke, G. Winter, F. Lidén, B. Cederwall, A. Johnson, R. Wyss, J. Nyberg, and G. Sletten, in *High Spin Physics and Gamma-Soft Nuclei*, edited by J.X. Saladin, R.A. Sorensen, and C.M. Vincent (World Scientific, Singapore, 1991), p. 381.
[18] L.C. Northcliffe and R.F. Schilling, Nucl. Data Sec. A **7**, 233 (1970).
[19] J.F. Ziegler and W.K. Chu, At. Data Nucl. Data Tables **13**, 463 (1974).
[20] J.F. Ziegler, J.P. Biersack, and U. Littmark, *The Stopping and Range of Ions in Solids* (Pergamon, New York, 1985).
[21] J. Lindhard, M. Scharff, and H.E. Schiott, K. Dan, Vidensk. Selsk., Mat-Fys. Medd. **33**, No. 14 (1963).
[22] S. Kalbitzer, H. Oetzmann, N. Grahmann, and A. Feuerstein, Z. Phys. A **278**, 223 (1976).
[23] A.E. Blaugrund, Nucl. Phys. **88**, 501 (1966).
[24] P. R. Bevington, *Data Reduction and Error Analysis for the Physical Sciences* (McGraw-Hill, New York, 1969).
[25] J.W. Holcomb, J. Döring, T. Glasmacher, G.D. Johns, T.D. Johnson, M.A. Riley, P.C. Womble, and S.L. Tabor, Phys. Rev. C **48**, 1020 (1993).
[26] F. Cristancho and K.P. Lieb, Nucl. Phys. **A486**, 353 (1988); F. Cristancho, K.P. Lieb, J. Heese, C.J. Gross, W. Fieber, Th. Osipowicz, S. Ulbig, K. Bharuth-Ram, S. Skoda, J. Eberth, A. Dewald, and P. von Brentano, Nucl. Phys. **A501**, 118 (1989).
[27] L. Funke, J. Döring, F. Dubbers, P. Kemnitz, E. Will, G. Winter, V.G. Kiptilij, M.F. Kudojarov, I. Kh. Lemberg, A.A. Pasternak, A.S. Mishin, L. Hildingsson, A. Johnson, and Th. Lindblad, Nucl. Phys. **A355**, 228 (1981).
[28] V.A. Wood, J. Döring, J.W. Holcomb, G.D. Johns, T.D. Johnson, M.A. Riley, G.N. Sylvan, P.C. Womble, and S.L. Tabor (unpublished).
[29] H.G. Price, C.J. Lister, B.J. Varley, W. Gelletly, and J.W. Olness, Phys. Rev. Lett. **51**, 1842 (1983).
[30] C.J. Lister, P. Chowdhury, and D. Vretenar, Nucl. Phys. **A557**, 361c (1993).
[31] R.F. Davie, D. Sinclair, S.S.L. Ooi, N. Poffé, A.E. Smith, H.G. Price, C.J. Lister, B.J. Varley, and I.F. Wright, Nucl. Phys. **A463**, 683 (1987).
[32] L.P. Ekström, G.D. Jones, F. Kearns, T.P. Morrison, A. Nilsson, P.J. Twin, R. Wadsworth, E. Wallander, and N.J. Ward, J. Phys. G **6**, 1415 (1980).
[33] D. Bucurescu, G. Constantinescu, M. Ivascu, N.V. Zamfir, and M. Avrigeanu, J. Phys. G **7**, 399 (1981).
[34] A. Dewald, U. Kaup, W. Gast, A. Gelberg, H. -W. Schuh, K.O. Zell, and P. von Brentano, Phys. Rev. C **25**, 226 (1982).
[35] S.L. Tabor, P.D. Cottle, C.J. Gross, U.J. Hüttmeier, E.F. Moore, and W. Nazarewicz, Phys. Rev. C **39**, 1359 (1989).
[36] C.J. Lister, B.J. Varley, W. Fieber, J. Heese, K.P. Lieb, E.K. Warburton, and J.W. Olness, Z. Phys. A **329**, 413 (1988).
[37] S.L. Tabor, Phys. Rev. C **34**, 311 (1986).
[38] S.L. Tabor, Phys. Rev. C **45**, 242 (1992).
[39] W. Nazarewicz, M.A. Riley, and J.D. Garrett, Nucl. Phys. **A512**, 61 (1990).